CONF-900926--4

UCRL-JC--105113

DE91 004197

The Role of Resonances in Strong-Field Multiphoton Processes

M.D. Perry and K.C. Kulander

RECEIVED
NOV 30 1990

This paper was prepared for submittal to the Proceedings of the International Conference on Multiphoton Processes (ICOMP V), Paris, France September 24-28, 1990.

October, 1990

Lawrence Livermore National Laboratory

This is a preprint of a paper intended for publication in a journal or proceedings. Since changes may be made before publication, this preprint is made available with the understanding that it will not be cited or reproduced without the permission of the author.

MASTER

DISTRIBUTION OF THIS DOCUMENT IS UNLIMITED

DISCLAIMER

This document was prepared as an account of work sponsored by an agency of the United States Government. Neither the United States Government nor the University of California nor any of their employees, makes any warranty, express or implied, or assumes any legal liability or responsibility for the accuracy, completeness, or usefulness of any information, apparatus, product, or process disclosed, or represents that its use would not infringe privately owned rights. Reference herein to any specific commercial products, process, or service by trade name, trademark, manufacturer, or otherwise, does not necessarily constitute or imply its endorsement, recommendation, or favoring by the United States Government or the University of California. The views and opinions of authors expressed herein do not necessarily state or reflect those of the United States Government or the University of California, and shall not be used for advertising or product endorsement purposes.

The Role of Resonances in Strong-Field Multiphoton Processes

M.D. Perry and K.C. Kulander

Laser Program, Lawrence Livermore National Laboratory,
P.O. Box 808, L-490, Livermore, California 94550

Resonantly-enhanced multiphoton ionization (REMPI) has been the subject of extensive experimental[1-5] and theoretical[6-10] study since the invention of the laser. Until recently, the overwhelming majority of REMPI research have been conducted at intensities less than 10^{12} W/cm^2. At these intensities, the strength of the applied field remains less than one percent of the atomic Coulomb field experienced by the outer electrons in a typical noble gas atom. In this regime, treatment of the applied field as a weak perturbation on the atomic system yields excellent agreement with experiment.[11] Here, we investigate the role of resonances in multiphoton ionization at much higher intensities, specifically, we examine the behaviour and influence of resonances as the strength of the applied field becomes a significant fraction of the atomic field.

The success of theories which connect only the ground atomic state to an outgoing dressed electron state[12,13] in predicting ionization rates[14] and (ATI) electron spectra[15] in this regime suggest that resonances to intermediate atomic states, if they occur during the laser pulse, do not significantly affect the ionization rate. Conversely, observations by Freeman, et. al.[16] and others[17] of fine structure in electron spectra produced by the above-threshold ionization (ATI) of xenon at 616 nm and observable changes in the overall ionization rate[18] suggest that intermediate resonances remain important even at intensities greater than 10^{14} W/cm^2. Such resonances may play an important role in the production of high-order harmonic radiation in strong fields.[19,20] Only by examining the behaviour of isolated states as a function of both laser intensity and frequency can the influence of the state be adequately determined.

Potentially, the energy distribution of electrons resulting from above-threshold ionization with "short" laser pulses is the most sensitive indicator of resonant enhancement. In this technique, resonant enhancement appears as an increase in the electron yield at a specific electron energy.[16] The energy of the electron in turn yields the intensity at the moment of ionization from the value of the unrecovered ponderomotive potential.[16,18,19] In principle, the ac Stark shift

and the relative strength of the resonance can then be directly determined. In practice, this technique requires pulses having a duration typically less than a few picoseconds and a combination of laser frequency and intensity sufficient to provide accurately measureable ponderomotive potentials. These requirements place a limit on the parameter space accessible with this technique.

Here, we present the results of experiments and calculations from a study of resonant enhancement from several isolated states in helium, krypton and xenon. We utilize the technique of short-pulse electron spectroscopy where applicable and also examine the ion yield as a function of both frequency and intensity.

The lasers used in these experiments are described in detail elsewhere.[21,22] Briefly, the system consists of a synchronously mode-locked dye laser amplified in a three-stage diffraction-filtered amplifier pumped by 70 psec 532 nm radiation obtained from an Nd:YAG regenerative amplifier. The system produces Fourier transform-limited, 800 fsec pulses over the range 560 to 620 nm with an energy per pulse of from one to five millijoules (depending upon wavelength). Second-harmonic radiation (280-310 nm) is obtained by type I conversion in a 5 mm thick KD*P crystal with a maximum conversion efficiency of 30%. The pulses are focused into low density target gas with fused silica lenses in focal geometries of $4<f/D<15$. At an f# of 5, and 300 nm, a slightly astigmatic spot of approximately 10 μm diameter is obtained resulting in a maximum intensity of 1×10^{15} W/cm^2.

The first series of experiments consist of measuring the absolute number of multiply charged ions of Kr and Xe as a function of both laser intensity and frequency using a time-of-flight spectrometer. While not as precise as short-pulse electron spectra (described later) for determining the effects of a large number of resonances, such measurements can produce accurate values of the AC Stark shift, the ionization rate and the excitation rate to an <u>isolated</u> intermediate state.

We first considered the case of nonresonant multiphoton ionization in xenon by tuning the laser throughout the range 284 to 300 nm. No significant resonant enhancement could be observed throughout this wavelength range. The absolute yield of multiply-charged xenon ions was then studied as a function of laser intensity at several selected wavelengths both to confirm the lack of resonant enhancement and determine the three-photon ionization cross section, $\sigma^{(3)}$. The ion yield at three of these wavelengths is shown as a function of peak laser intensity, I_0, in figure 1. Although there is clear evidence of resonant behaviour in the yield of Kr^+, the yield of Xe^+ and Xe^{2+} is essentially independent of wavelength. The curvature in the ion yield curves above approximately 3×10^{13} W/cm^2 is due to saturation of the ionization probability. Specifically, as the

ionization probability approaches unity, target atoms become depleted throughout the focal volume. Further contribution to the ion yield then comes from the expanding focal volume which grows as $I_0^{3/2}$.

The production of multiply-charged ions was analyzed using a kinetic model developed previously.[21] The model includes both direct and sequential ionization leading to the production of the higher charge states. However, no evidence is found here to suggest a significant contribution of direct processes to the formation of multiply charged ions. Table 1 presents the measured cross-sections for the case of nonresonant multiphoton ionization at 293 nm. The cross sections presented are obtained using an ionization rate given by lowest-order perturbation theory, $W(\mathbf{r},t)=\sigma^{(K)}I^K(\mathbf{r},t)$, where K is the minimum number of photons required to ionize the atom.

TABLE I. Multiphoton ionization cross sections.

Species	Number of photons	Cross section ($cm^{2K} sec^{K-1}$)	Saturation intensity (W/cm^2)
Xe	3	$(2\pm1)\times10^{-83}$	3×10^{13}
Kr	4	$(8\pm4)\times10^{-116}$	4.5×10^{13}
Xe^+	6	$(5\pm3)\times10^{-180}$	5.8×10^{13}

Considering the observed deviations from lowest-order perturbation theory in the same intensity range but longer wavelength,[14] the validity of the cross-sections in Table I may seem questionable. This was investigated by examining the electron spectra in the same intensity range. Although not presented here, at low intensities, essentially all of the ions of Xe^+ are produced in the $^2P_{3/2}$ ground state.[23] This corresponds to the lowest-order pathway since an additional photon is required to produce an ion in the $^2P_{1/2}$ state. As the intensity is increased, electrons corresponding to the production of the ion in the $^2P_{1/2}$ state can be observed along with the appearance of the first above-threshold peak (s=1) for the $^2P_{3/2}$ state. The intensity at which these four photon processes is, within experimental uncertainty, the same. As the intensity is increased to 8×10^{13} W/cm^2, the five photon processes corresponding to $^2P_{3/2}$ (s=2) and $^2P_{1/2}$ (s=1) become observable. However, the yield of these higher order processes is less than 10% of the threshold ionization (s=0) yield. Hence, the overall ionization rate should be well described by a third-order process. This conclusion is well supported by calculations using a modified Keldysh-Faisal-Reiss type theory[14] and a numerical solution of the time-dependent Schrodinger equation.[24]

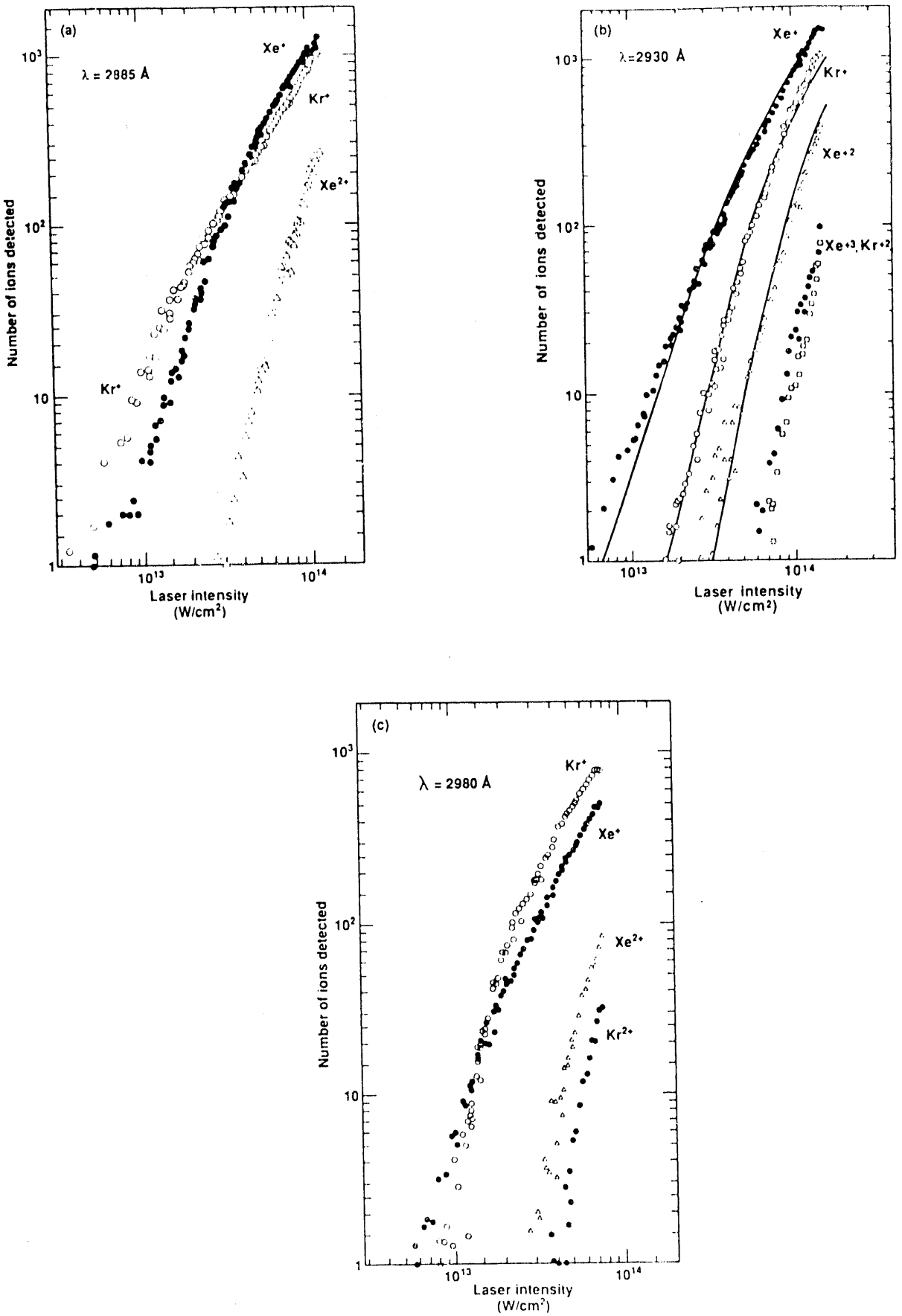

FIG. 1. Absolute ion yield of krypton ($P_{Kr} = 1.4 \times 10^{-6}$ Torr) and xenon ($P_{Xe} = 1.6 \times 10^{-6}$ Torr) as a function of peak laser intensity at selected laser frequencies: (a) 288.5 nm, near resonance B of Fig. 10; (b) 293 nm, nonresonant; (c) 298 nm, near resonance C.

Four-photon resonantly-enhanced ionization of krypton

Resonant enhancement in the production of Kr^+ at 288.5 and 298.0 nm is apparent in figures 1a and 1c, respectively. At 288.5 nm, the ion yield of krypton is above that of xenon at low intensity but falls below that of xenon at higher intensities. This behaviour can be explained by the laser being three-photon resonant with an intermediate state at low intensity. As the intensity rises, the state is shifted out of resonance resulting in a corresponding drop in the ionization rate. In contrast, at 298.0 nm, the yield of Kr^+ starts out below the yield of Xe^+ but rises quickly above the yield of Xe^+ at an intensity of approximately 1.5×10^{13} W/cm^2. In this case, the laser could be initially nonresonant, then, as the intensity increases, the field shifts an intermediate state into resonance. This state which is both shifted and broadened by the field then remains in resonance until saturation is achieved. Finally, at 293.0 nm, the Kr^+ signal shows no evidence of resonant enhancement and exhibits an $I^{4.0 \pm 0.3}$ dependence, consistent with nonresonant, four-photon ionization.

To further examine the interpretation of the ion yield data, we measured the yield of Kr^+ as a function of laser wavelength at several values of the laser intensity. The results at 0.6, 1.4, and 3.0×10^{13} W/cm^2 are shown in figure 2. Several resonances are apparent. More detailed data on resonance "B" is presented in Figure 3. Reference to the krypton energy level diagram[25] indicates that several states can be accessed by dipole-allowed, three-photon transitions over the range of laser frequency considered here.

The states producing resonant enhancement have been identified on the basis of an extrapolation of the position of the resonance to the limit of now applied field. In cases where this extrapolation does not result in an unambiguous identification, the dominate intermediate state was identified on the basis of an estimate of the three-photon matrix element between the ground and excited state using. This estimate consisted of evaluating a truncated sum of published single-photon matrix elements[26] connecting states along the dominate pathway.

From these calculations and extrapolated resonance positions, the observed resonant enhancement arises from: (A) a combination of the $4d'[3/2]_1$ and $5d[7/2]_3$; (B) a combination of the $4d'[5/2]_3$ and the $5d[1/2]_1$; (C) a combination of the $4d[3/2]_1$ and the $6s[3/2]_1$; (D) the $4d[5/2]_3$; (E) the $4d[7/2]_3$; and (F) the $4d[1/2]_1$. The level designations are given in abbreviated $j_c l$ notation in which a prime is used to donate states with a $P_{1/2}$ core. Configuration mixing (particularly among the 4d' and 5d states) may be strong, making such single level designations invalid.

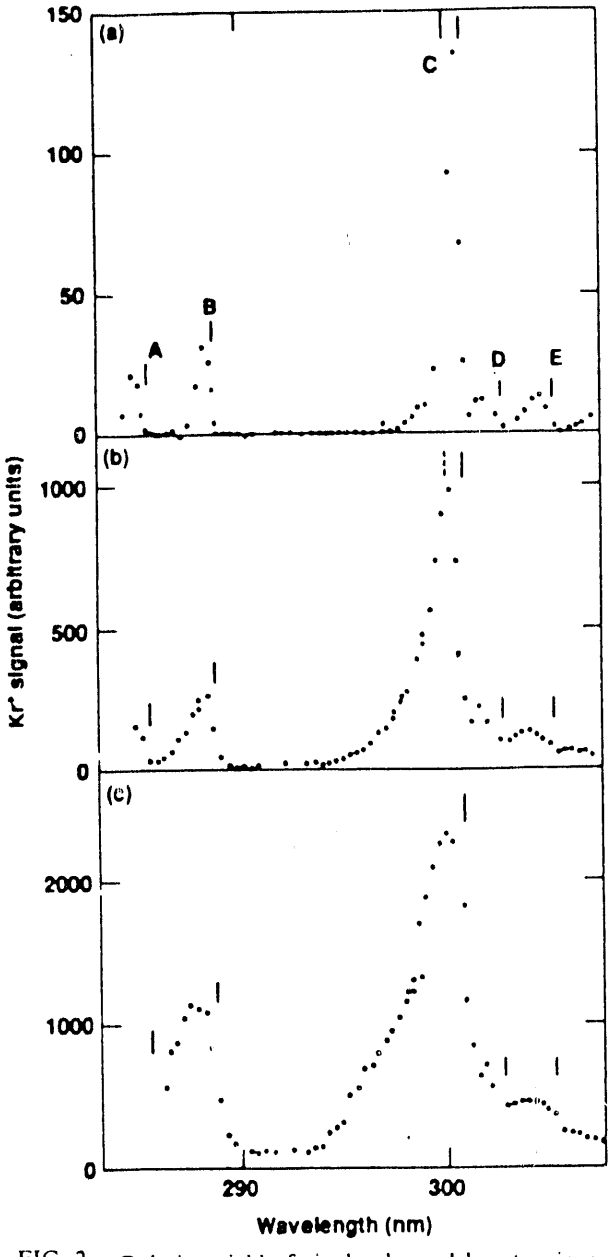

FIG. 2. Relative yield of singly charged krypton ions as a function of laser wavelength at various peak intensities: (a) $I_0 = 6\times10^{12}$ W/cm^2, (b) $I_0 = 1.4\times10^{13}$ W/cm^2, (c) 3×10^{13} W/cm^2. Vertical lines mark the field-free positions of dipole allowed, three-photon resonances in neutral Kr

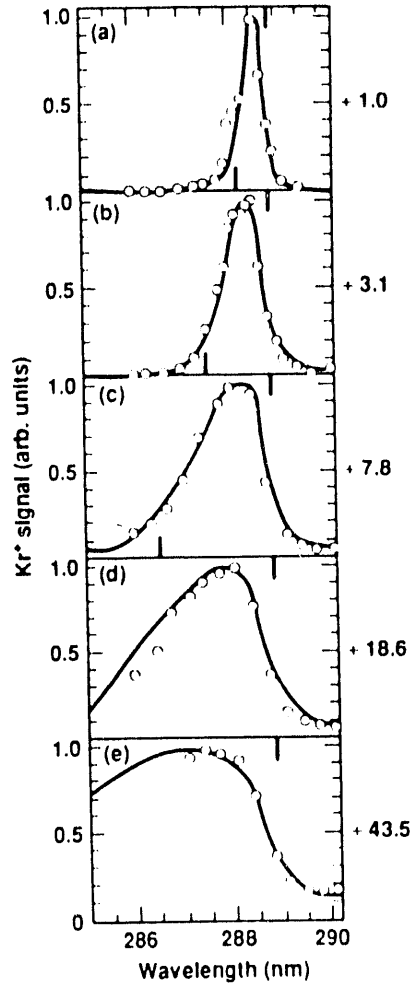

FIG. 3. Spectral profile of resonance B, attributed primarily to the $4d'[\frac{3}{2}]_3$, for various peak intensities: (a) $I_0 = 7.4\times10^{12}$ W/cm^2, (b) $I_0 = 1.5\times10^{13}$ W/cm^2, (c) $I_0 = 2.7\times10^{13}$ W/cm^2, (d) $I_0 = 4.5\times10^{13}$ W/cm^2, (e) $I_0 = 7.8\times10^{13}$ W/cm^2.

Furthermore, the estimates of the three-photon matrix elements and level designations given above follow from knowledge of the wave functions in the absence of an applied field. In the case of strong applied fields, the coupling of the excited electron to the field can be stronger than the spin-orbit interactions which give rise to the level splittings and consequent coupling schemes. Hence, such level designations and strength estimates must be treated with caution and can only be accepted when supported by detailed theoretical calculations which treat the coupled atom-field system. Such calculations have recently been performed for krypton under the conditions of this experiment.[27] The results of these calculations for the three-photon Rabi rate, ac Stark shift and photoionization rate of the excited state for resonances B and C are compared with the experimentally measured quantities in Table II. A detailed description of the calculational procedure can be found in reference 27 and the method by which the atomic parameters are extracted from the experimental data can be found in reference 23.

TABLE II. Measured atomic parameters in the four-photon ionization of Kr

Resonance Designation	Identification	Three-photon Rabi Coefficient (cm^6-sec)	Net ac Stark Shift (meV/TW-cm^2)	Ionization cross section (10^{18} cm^2)
Experiment				
B	$4d'[5/2]_3$	$(2\pm0.7)\times10^{-69}$	3.9 ± 0.7	3.0 ± 0.6
C	$4d\,[3/2]_1$	$(8\pm4)\times10^{-69}$	8.0 ± 0.8	8 ± 1
Calculated[27]				
B	$4d'[5/2]_3$	3.2×10^{-70}	6.9	10.6
C	$4d\,[3/2]_1$	4.1×10^{-69}	8.0	3.9

Resonantly-enhanced above-threshold ionization of helium

Helium is of particular interest for several reasons. First, its simple structure permits detailed calculations. Second, it provides two strong intermediate resonances, $1s^2+5h\omega \rightarrow 1s2p$ and $1s^2+6h\omega \rightarrow 1s3d$, which are well separated from other states and bound by at least 1.5 eV. This removes much of the ambiguity associated with examining resonances to states near the continuum.[16]

Photoelectrons resulting from above-threshold ionization are born with a kinetic energy,[28]

$$E_e=(K+S)h\omega - IP(I) = (K+S)h\omega - IP(0) - U_p(I) \qquad (1)$$

where K is the minimum number of photons which must be absorbed to ionize the

atom in the absence of the field, and S is the number of additional (ATI) photons absorbed. The ionization threshold, IP, is intensity dependent to account for the quiver energy of the newly freed electron in the field. This quiver or "ponderomotive" energy is given by, $U_p=e^2A^2/(4mc^2)=9.33\times10^{-14}\ I\lambda^2$ (eV) where I is the laser intensity in W/cm^2 and λ is the wavelength of the laser light in microns. The difference in the dynamic Stark shifts of the atomic and ionic ground states is not included in eq. 1 since it is negligible relative to the quiver energy of the electron.

If the duration of the laser pulse is shorter than the time required for the electron to leave the laser focus, then the conversion of potential to kinetic energy is incomplete and results in an intensity dependent deficit in the kinetic energy. In the limit that the pulse is infinitely short, the electron energy detected is equal to the energy with which the electron is born (eq. 1), and hence *records the intensity present at the moment of ionization* The short pulse regime is approached with subpicosecond lasers.[16,29]

The electron spectrometer used in these experiments collects all electrons emitted within the 2π solid angle in the direction of the microchannel plate detector.[30] The energy of a given photoelectron is determined by its time of flight down a 50 cm drift tube. The spectrometer was calibrated utilizing the photoelectron spectrum resulting from the above-threshold ionization of xenon and helium at 532 nm with long (70 psec) pulses.

The ultraviolet pulses were focused into low density helium gas with a 45 mm focal length fused silica lens (f#=5) to a slightly astigmatic spot of approximately 10 μm diameter. The experiments were conducted in a range of helium pressure between 4×10^{-7} and 4×10^{-6} Torr. The pressure was decreased as the laser intensity was increased in order to avoid space charge distortion of the spectrum.[31] A typical time of flight spectrum at a peak laser intensity of 4×10^{14} W/cm^2 and 291 nm is shown in figure 4. Electrons corresponding to the absorption of seven (s=1), eight (s=2), and nine (s=3) photons can be observed at this intensity. At higher intensities, electrons corresponding to the absorption of ten photons could be observed. Electrons corresponding to threshold ionization (s=0) could be produced only from regions of intensity less than 1.2×10^{14} W/cm^2 (eq. 1) and are not observed at this wavelength. Electrons corresponding to s=1 clearly come in two distinct energy groups indicating electrons produced at different intensities.

Figure 5 contains data taken at 281.5 nm in the region from 2 - 9 eV for several values of peak laser intensity. The averaged spectra shown in figures 5 a-e are acquired by sorting the spectra of several hundred laser shots into narrow bins of differing electron yield. Since the yield is a strong function of laser intensity, this

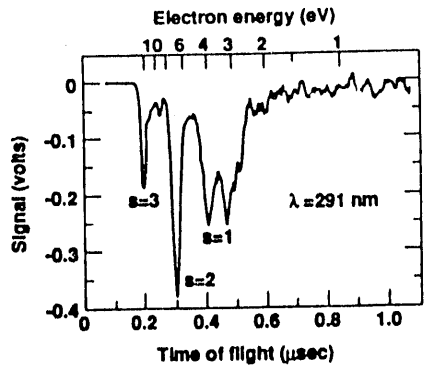

FIG. 4. Electron spectrum resulting from the above-threshold ionization of helium at 291 nm and a peak intensity of 4×10^{14} W/cm^2.

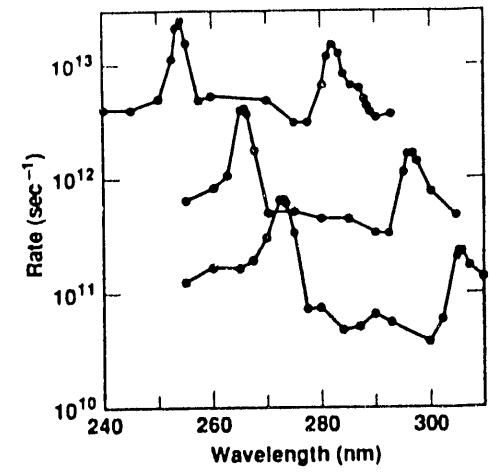

FIG. 6. Ionization rates for helium as a function of laser wavelength obtained from the numerical solution of the time-dependent Schrödinger equation at 2×10^{14}, 3×10^{14}, and 5×10^{14} W/cm^2.

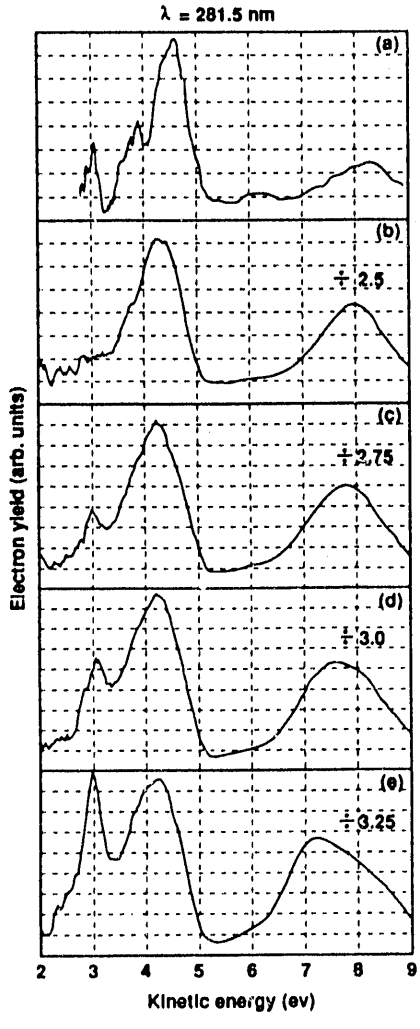

FIG. 5. Electron-energy distribution obtained at 281.5 nm ($s=1$ and $s=2$ peaks only) at various laser intensities (units of 10^{14} W/cm^2): (a) $I_0=3.1$, (b) 3.6, (c) 3.8, (d) 4.3, and (e) 4.4. Data below 3.5 eV in (a) are not statistically significant. The change in the vertical scale is given by the factor at the right-hand side of each figure.

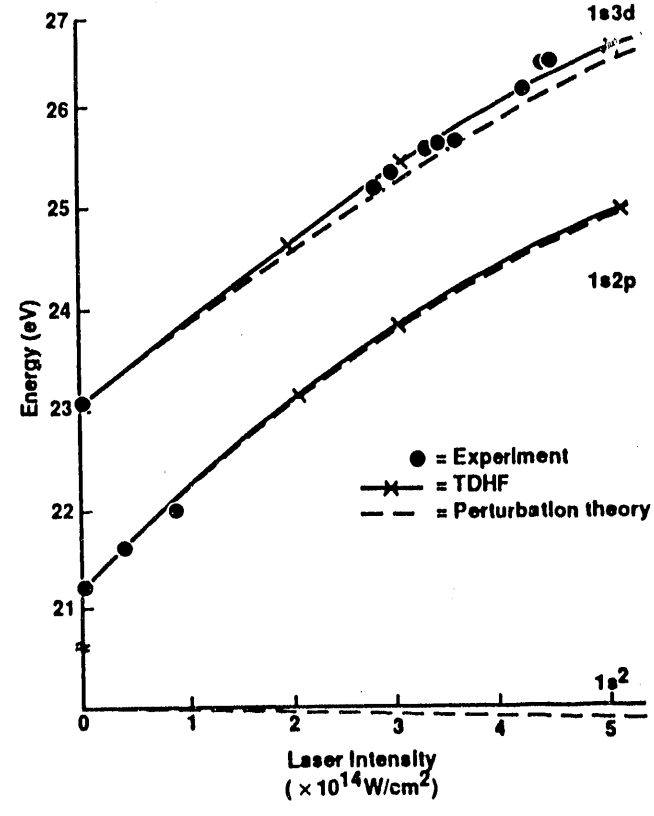

FIG. 7. Energy of states arising from the $1s2p$ and $1s3d$ field-free singlet states of helium as a function of laser intensity. The dashed curve originating at zero energy for the $1s^2$ emphasizes the shift of the ground state to lower energy with increasing intensity.

method results in sets of spectra averaged over a narrow intensity interval.[32] The 2-9 eV region covers the s=2 peak near 7.5 eV and the s=1 peak between 2.5 and 4 eV. These peaks are clearly shifted from the field-free positions of 6.24 and 10.6 eV which would have been obtained with 'long' laser pulses. At the lower intensities, the electron spectrum exhibits single peaks corresponding to the the absorption of seven (s=1) and eight (s=2) photons. As the laser intensity increases, some of the s=1,2 electrons are observed with decreasing energy. At a peak intensity of 4×10^{14} W/cm^2, a clear second peak appears which is apparently part of the s=1 peak. Similar substructure in the s=2 peak is observed by acquiring the s=2 electrons under higher energy resolution (not shown). As the intensity is raised further, the yield of electrons to this secondary peak increases but its position does not shift towards lower energy as does the primary part of the s=1 peak.

The secondary peak apparently arises from a region of laser intensity appropriate to shift a state into resonance with an integral number of 4.4 eV photons (281.5 nm). The ionization probability in this region is enhanced relative to the nonresonant probability by the intermediate resonance. Since the intensity at which the electron is produced determines its energy (eq. 1), those electrons produced from resonant enhancement will always appear at the same energy regardless of the value of the peak laser intensity.

Examination of the positions of the field-free singlet states in helium suggests that the enhancement observed in the s=1 peak is due to a six photon resonance to the 1s3d state. At 281.5 nm, this state would have to be shifted towards higher energy by 3.3 eV to be resonant. This was confirmed by acquiring electron spectra at several wavelengths in the range 280 to 297 nm. Longer wavelength light requires less of a shift and results in the appearence of the resonance at lower laser intensity (fig. 6). Hence, the position of the resonance as a function of intensity can be traced by tuning the laser frequency. At the shortest wavelengths, a second resonance corresponding to five-photon excitation of the 1s2p was observed.

To provide further insight to the experimental data, we developed a nonperturbative theoretical description of helium subjected to these strong fields. We solve the atom-field Schrodinger equation by direct numerical integration for an adiabatic pulse. The laser pulse rises linearly over several optical cycles and is then held constant at the prescribed intensity. During the constant intensity interval, the atom is found to decay exponentially thereby giving an ionization rate for the particular intensity and wavelength. The model of the helium atom used here[33] allows only one of the two electrons to interact with the field. The second electron is held frozen in its ground (Hartree-Fock) orbital.

We performed a series of calculations at selected values of the laser intensity as a function of wavelength between 240 and 320 nm. Two strong features are evident (fig. 6), the strongest is a result of five-photon resonance with a state arising from the 1s2p and the other a result of six-photon excitation of a state arising from the 1s3d. Projection of these wavefunctions onto the field-free states shows that these states are no longer pure 1s2p (1s3d) but are strongly mixed by the field. Both states shift towards higher energy with increasing laser intensity and exhibit a width which is dominated by the short lifetime of these excited states at intensities above 10^{14} W/cm^2.

The calculated and experimental energy of the 1s2p and 1s3d states is shown as a function of laser intensity in Figure 7. The solid curve represents the results of our numerical solution to the Schrodinger equation. For comparison, we have also carried out a lowest order perturbation theory calculation (corrected to account for the changing laser wavelength) for the energy of both the ground and excited states (dashed curve). Both the numerical and perturbation theory calculations of the resonance positions reproduce the experimental data within a few percent over the range of intensity investigated.

Ionization rates obtained from the electron yield to each ATI peak were generally found to be slightly higher than our time-dependent Hartree-Fock (TDHF) calculated rates but lower than those from our modified version[14] of the Keldysh-Reiss-Faisal (KRF) theory. Specifically, at an intensity of 3×10^{14} W/cm^2 and wave length of 294 nm, we calculate an ionization rate of 1.5×10^{12} sec^{-1} for six-photon resonant (1s3d), seven-photon (s=1) ionization, while experiment yields a value of $(3\pm1)\times10^{12}$ sec^{-1}. For "non-resonant" seven-photon ionization at this intensity and wavelength, we calculate rates of $(3\pm1)\times10^{11}$ sec^{-1} (TDHF) and 2.5×10^{12} sec^{-1} (KRF), but measure a rate of $(1.5\pm0.8)\times10^{12}$ sec^{-1}. The apparent uncertainty in the numerical (TDHF) calculations for the nonresonant ionization is a result of some definite, but comparatively weak, structure between the two main resonances. We attribute this weak structure to six photon resonances through the Rydberg states, a feature which may become more pronounced at lower intensities. It is important to note that the primary part of the s=1 peak in the electron yield discussed earlier (figure 5) may in fact be the result of resonances to these Rydberg states.

In conclusion, we have demonstrated that intermediate multiphoton resonances can play a significant role in above-threshold ionization even at intensities exceeding 10^{14} W/cm^2. By combining measurements of ion and (where possible) electron spectra as a function of both laser frequency and intensity, the ac Stark shift, multiphoton excitation rates and photoionization cross sections of

various intermediate states can be determined even in the strong-field regime. Detailed perturbation theory calculations are in good agreement with the experimental results for the multiphoton ionization of krypton and xenon at intensities up to 5×10^{13} W/cm^2 in the range 284-300 nm. At higher intensities, (up to 4×10^{14} W/cm^2), a numerical solution of the time-dependent Schrodinger equation for a single-electron atomic model provides ionization rates and resonance positions which are in good agreement with experimental results in the above-threshold ionization of helium.

References

1. J. Morellec, D. Normand, and G. Petite, Phys. Rev. A, **14**, 300 (1976).
2. L.A. Lompre, G. Mainfray, C. Manus, and J. Thebault, Phys. Rev. A, **15** 1604 (1977); L.A. Lompre, G. Mainfray, and C. Manus, J. Phys. B, **13**, 65 (1980).
3. G.C. Bjorklund, R.R. Freeman, and R.H. Storz, Opt. Comm. ,**31**, 47 (1979).
4. R.N. Compton, J.C. Miller, A. Carter and P. Kruit. Chem. Phys. Lett.,**71**, 87 (1980).
5. J. Bokor, J. Zavelovich, and C.K. Rhodes, Phys. Rev. A, **21**, 1455 (1980).
6. U. Eichmann, Y. Zhu, and T.F. Gallagher, J. Phys. B, **20**, 4461 (1987).
7. A. Georges and P. Lambropoulos, Phys. Rev. A, **15**, 727 (1977); P. Lambropoulos, Adv. Electronics and Electron Physics, **54**, 191 (1980).
8. Y. Gontier and M. Trahin, J. Phys. B, **13**, 259 (1980).
9. P. Zoller, J. Phys. B, **15**, 2911 (1982).
10. M. Crance, J. Phys. B, **13**, 101 (1980).
11. F.H.M. Faisal, *Theory of Multiphoton Process*, (Plenum, New York, 1987).
12. L.V. Keldysh, Sov. Phys. JETP, **20**, 1307 (1965).
13. F.H.M. Faisal, J. Phys. B, **6**, L89 (1973); H.R. Reiss, Phys. Rev. A, **22**, 1786 (1980).
14. M.D. Perry, A. Szoke, O.L. Landen, and E. M. Campbell, Phys. Rev. Lett., **60**, 1270 (1988); S.L. Chin, C. Rolland, P.B. Corkum, and P.Kelly, Phys. Rev. Lett., **61**, 153 (1988).
15. P.H. Bucksbaum, M. Bashkansky, and D.W. Schumacher, Phys. Rev. A, **37**, 3615 (1988).
16. R.R. Freeman, P.H. Bucksbaum, H. Milchberg, S. Darack, D. Schumacher, and M.E. Geusic, Phys. Rev. Lett., **59**, 1092 (1987).
17. H.G. Muller, H.B. van Linden van de Heuvell, P. Agostini, G. Petite, A. Antonetti, M. Franco, and A. Migus, Phys. Rev. Lett., **60**, 565 (1988).
18. O.L. Landen, M.D. Perry and E.M. Campbell, Phys. Rev. Lett, **59**, 2558 (1987).
19. M. Ferray, A. L'Hullier, X.F. Li, L.A. Lompre, G. Mainfray, and C. Manus,

J. Phys. B, **21**, L31 (1988).

20. K.C. Kulander and B.W. Shore, Phys. Rev. Lett., **62**, 524 (1989).
21. M.D. Perry, O. Landen, A. Szoke, and E.M. Campbell, Phys. Rev. A, **37**, 747 (1988).
22. M.D. Perry, O.L. Landen, J. Weston, and R. Ettelbrick, Opt. Lett., **14**, 42 (1989).
23. M.D. Perry and O.L. Landen, Phys. Rev. A, **38**, 2815 (1988).
24. K.C. Kulander, Phys. Rev. A, **38**, 778 (1988).
25. V. Kaufman and C.J. Humphreys, J. Opt. Soc. Am. **59**, 1614 (1969).
26. M. Aymar and M. Coulombe, At. and Nuc. Data Tables, **21**, 537 (1978).
27. X. Tang, P. Lambropoulos, A.L'Huillier,and S. Dixit, Phys. Rev. A, **40**, 7026 (1989).
28. A. Szoke, J. Phys. B, **18**, L427 (1985).
29. T.S. Luk, T. Graber, H. Jara, U. Johann, K. Boyer, and C.K. Rhodes, J. Opt. Soc. Amer. B, **4**, 847 (1987).
30. P. Kruit and F.H. Read, J. Phys. E, **16**, 313 (1983).
31. M. Crance, J. Phys. B, **19**, L267 (1986).
32. M.D. Perry, O.L. Landen, and A. Szoke, J. Opt. Soc. Amer. B, **6**, 344 (1989).
33. K.C. Kulander, Phys. Rev. A, **36**, 2726 (1987).

*This work was performed under the auspices of the U.S. Department of Energy by Lawrence Livermore National Laboratory under contract No. W-7405-Eng-48.

END

DATE FILMED

12 / 11 / 90